Development of Effective Connectome from Infancy to Adolescence

Guoshi Li[1[0000-0002-8984-4722]], Kim-Han Thung[1], Hoyt Taylor[1], Zhengwang Wu[1], Gang Li [1], Li Wang[1], Weili Lin[1], Sahar Ahmad[1], and Pew-Thian Yap[1*[0000-0003-1489-2102]]

[1] Department of Radiology and Biomedical Research Imaging Center (BRIC), University of North Carolina at Chapel Hill, Chapel Hill, USA
ptyap@med.unc.edu

Abstract. Delineating the normative developmental profile of functional connectome is important for both standardized assessment of individual growth and early detection of diseases. However, functional connectome has been mostly studied using functional connectivity (FC), where undirected connectivity strengths are estimated from statistical correlation of resting-state functional MRI (rs-fMRI) signals. To address this limitation, we applied regression dynamic causal modeling (rDCM) to delineate the developmental trajectories of effective connectivity (EC), the directed causal influence among neuronal populations, in whole-brain networks from infancy to adolescence (0-22 years old) based on high-quality rs-fMRI data from Baby Connectome Project (BCP) and Human Connectome Project Development (HCP-D). Analysis with linear mixed model demonstrates significant age effect on the mean nodal EC which is best fit by a "U" shaped quadratic curve with minimal EC at around 2 years old. Further analysis indicates that five brain regions including the left and right cuneus, left precuneus, left supramarginal gyrus and right inferior temporal gyrus have the most significant age effect on nodal EC ($p < 0.05$, FDR corrected). Moreover, the frontoparietal control (FPC) network shows the fastest increase from early childhood to adolescence followed by the visual and salience networks. Our findings suggest complex nonlinear developmental profile of EC from infancy to adolescence, which may reflect dynamic structural and functional maturation during this critical growth period.

Keywords: Functional MRI, Effective Connectivity, Brain Networks.

1 Introduction

The human brain development undergoes a unique and dynamic process from birth through adolescence, encompassing remarkable structural and functional changes. It has been well recognized that the period immediately after birth offers a critical time window for the establishment of both structural and functional architectures through a series of complex neurobiological processes including synaptogenesis, myelination, and axonal and synaptic pruning [1, 2]. Alongside with the neural substrate modifications, functional brain networks, revealed by resting-state functional MRI (rs-fMRI),

start to develop in a sequential, coordinated and hierarchical manner where the primary sensory systems (visual, sensorimotor and auditory networks) develop first and exhibit adult-like topologies in full-term newborns [3]. Adverse early life events could impose a long-lasting effect on brain network function by disrupting critical developmental process, resulting in developmental disorders with clinical presentations during childhood and later stages of life [2, 4].

The maturation and refinement of structural and functional brain networks continue from infancy to childhood and adolescence, another critical period for development. It has been shown that the brain's functional networks switch from an anatomical- dominant structure to a distributed architecture with elevated connectivity of the network hub [5, 6], indicating enhanced functional integration during development. Paralleled with the maturation of functional organization, children begin to develop cognitive, emotional and social abilities including self-awareness, autobiographical memory and moral judgement [7]. Thus, it is of great importance to delineate the developmental trajectory of the functional organization from infancy to adolescence for both standardized assessment of individual growth and early detection of diseases.

The development of large-scale functional networks has been well described in infancy [3], childhood and adolescence [8, 9] using fMRI-based functional connectivity (FC). For example, studies found increased FC within the default mode network (DMN) in older children than in younger children [8]. However, it should be noted that FC, defined as the statistical correlation of blood-oxygen-level-dependent (BOLD) signals, represents undirected synchronizations rather than directed causal influence (i.e., effective connectivity). As effective connectivity (EC) builds on a generative model of neural interaction, it can potentially provide more mechanistic insights underlying cognitive development [10].

Existing developmental studies based on EC networks is scare, partially due to the high computational burden associated with EC computation, especially in large-scale networks. Indeed, traditional EC models such as Dynamic Causal Modeling (DCM) are computationally intensive and usually restricted to small networks with a few brain regions [11]. Fortunately, such limitations have been largely overcome with the introduction of regression DCM (rDCM; [12-14]) which allows the construction of EC networks in large-scale brain-wide systems. In this study, we applied rDCM to a high-quality rs-fMRI dataset from BCP and HCP-D projects to delineate the developmental trajectory of effective connectome from infancy to adolescence.

2 Methods

2.1 Participants

We utilized rs-fMRI data from the BCP [15] and HCP Development (HCP-D; [16]). The rs-fMRI data included 318 subjects (158 females/160 males; age: 16 days-22 years) with a total of 428 scans (longitudinal scans in BCP). The BCP data was processed using an infant-dedicated pipeline [17] and the HCP-D data was processed by the HCP pipeline [18]. Regional averaged BOLD time series were extracted using the Desikan-Killiany atlas [19] with 68 cortical regions of interest (ROIs) grouped into six functional

networks (visual, somatomotor, salience, limbic, frontoparietal control, and default mode [20]).

2.2 The Original DCM

The original DCM uses a bilinear state model [11]:

$$\dot{x}(t) = [A + \sum_k B^k u_k(t)]x(t) + Cu(t) \tag{1}$$

where $x(t)$ denotes the hidden neuronal states for multiple brain regions, $u(t)$ represents exogenous experimental input, and the matrix C models the influence of external inputs on neuronal activity. A is the baseline EC and B^{k} represents the modulation on EC due to the input $u_{\mathrm{k}}(t)$. DCM employs a biophysical hemodynamic model to translate the regional neural activity $x_{\mathrm{i}}(t)$ to observed BOLD response $y_{\mathrm{i}}(t)$ [11].

$$\frac{ds_i(t)}{dt} = x_i(t) - \kappa s_i(t) - \gamma(f_i(t) - 1) \tag{2}$$

$$\frac{df_i(t)}{dt} = s_i(t) \tag{3}$$

$$\tau \frac{dv_i(t)}{dt} = f_i(t) - v_i^{\frac{1}{\alpha}}(t) \tag{4}$$

$$\tau \frac{dq_i(t)}{dt} = \frac{f_i(t)}{\rho}\left[1 - (1-\rho)^{1/f(t)}\right] - \frac{q_i(t)}{v_i(t)} v_i^{\frac{1}{\alpha}}(t) \tag{5}$$

where $s_{\mathrm{i}}(t)$ is the vasodilatory signal, $f_{\mathrm{i}}(t)$ is the blood flow, $v_{\mathrm{i}}(t)$ is the blood volume and $q_{\mathrm{i}}(t)$ is the deoxyhemoglobin content. κ is the rate of decay, γ is the rate of flow-dependent elimination, τ is the hemodynamic transit time, α is the Grubb's exponent and ρ is the resting oxygen extraction. The BOLD response is calculated as:

$$y_i(t) = v_0(k_1(1 - q_i(t)) + k_2(1 - q_i(t)/v_i(t)) + k_3(1 - v_i(t))) \tag{6}$$

where v_0 is the resting blood volume fraction, and k_1, k_2 and k_3 are the intravascular, concentration and extravascular coefficients, respectively. DCM then estimates the parameters A, B_{k} and C based on fMRI data.

2.3 The Regression DCM

Regression DCM is a novel variant of DCM [12-14]. To achieve high computational efficiency, rDCM makes several simplifications from the original DCM: (1) employing a linear DCM model (i.e., no modulation component); (2) converting the linear DCM equations from the time domain to the frequency domain using Fourier transformation; (3) replacing the nonlinear hemodynamic model with a linear hemodynamic response function (HRF); and (4) assuming partial independence between connectivity parameters. With such assumptions, rDCM treats model inversion in DCM as a special case of Bayesian linear regression problem, leading to the following likelihood function [14]:

$$\rho(y|\theta,\tau,X)=\prod_{r=1}^{R}N(Y_r;X\theta_r,\tau_r^{-1}I_{N\times N})$$

$$Y_r=(e^{2\pi i\frac{m}{N}}-1)\frac{\hat{y}_r}{T} \tag{7}$$

$$X=[\hat{y}_1,\hat{y}_2,\dots\hat{y}_R,\hat{h}\hat{u}_1,\hat{h}\hat{u}_2,\dots,\hat{h}\hat{u}_K]$$

$$\theta_r=[a_{r,1},a_{r,2},\dots a_{r,R},c_{r,1},c_{r,2},\dots c_{r,K}]$$

where y_r is the measured BOLD signal in region r, Y_r is the Fourier transformation of the temporal derivative of the BOLD signal, X is the design matrix, u_k represents the k_{th} experimental input (hat symbol indicates discrete Fourier transform), θ_r is the vector of parameters (connection parameters $a_{r,1}$, $a_{r,2}$,… $a_{r,R}$ and all driving input parameters $c_{r,1}$, $c_{r,2}$,… $c_{r,K}$ to region r). Also, τ_r represents the noise precision parameter for region r and I_{NXN} is an identity matrix. Using the likelihood function (7), rDCM efficiently estimates the parameters by iteratively updating a set of analytical Variational Bayes (VB) equations [14]. We focused EC estimation on the most pronounced edges based on FC [12, 14]. Specially, we averaged the FC matrices of all 428 scans and retained the strongest edges that have a FC value of greater than 0.4; weaker edges were removed.

2.4 Statistical Analysis

To characterize the influence of EC on nodes, we defined three nodal metrics: (1) net nodal EC, (2) excitatory nodal EC, and (3) inhibitory nodal EC. The net nodal EC is computed as the summation of all incoming EC to a particular node, while excitatory (inhibitory) nodal EC is calculated as the summation of all incoming excitatory (inhibitory) EC to a particular node. To quantify the effects of age on nodal EC, we used a linear mixed model [8] which can characterize the age- related continuous change. Given the potential linear or quadratic effects of age, we considered both a linear model and a quadratic model [8]. The linear model is defined as:

$$Y_{ij}=\beta_0+b_i+(\beta_{age}+b_{age,i})age_{ij}+\beta_{sex}Sex_i+\varepsilon_{ij},\ i=1,2,\dots,N \tag{8}$$

The quadratic model is defined as:

$$Y_{ij}=\beta_0+b_i+(\beta_{age1}+b_{age,i1})age_{ij}+(\beta_{age2}+b_{age,i2})age^2+\beta_{sex}Sex_i+\varepsilon_{ij},\ i=1,2,\dots, \tag{9}$$

where Y_{ij} represents the measurement of subject i at the jth scan, β_0 is the fixed intercept, bi the random effect on intercept, β_{age} denotes the fixed age effect, $b_{age,\ i}$ represents the random effect on age, and ε_{ij} is the residual. We used Akaike information criterion (AIC) value to select the best fit model [8]. Also, we divided the subjects into five different age groups: (1) Neonatal (0-0.5 year); (2) Late infancy (0.5-1 year); (3) Early childhood (1-6 years); (4) Late childhood (6-12 years) and (5) Adolescence (12-22 years) [21]. Comparison on nodal EC between different age groups was conducted by a two-sample t-test. Multiple comparisons were corrected by using the false discovery rate (FDR) method with $q < 0.05$.

3 Results

3.1 Nonlinear Evolution of EC from Infancy to Adolescence

The EC evolves from infancy to adolescence in a nonlinear fashion. The average EC among neonatal, late infancy and adolescence is showed in Fig. 1A, B, and C, respectively. We observed that for all three developmental phases, the EC exhibits modular structure where stronger EC edges exist within the same network than between different networks, similar to a previous DCM study [22]. Visual examination indicates the excitatory EC reduces from neonatal to late infancy and increases in adolescence (compare the yellow edges among Fig. 1A, B and C), while the inhibitory EC heightens from neonatal to late infancy and reduces in adolescence (compare the black edges among Fig. 1A, B and C). Such observation is confirmed by the summary plot of the average net nodal EC (Fig. 1D). The net nodal EC decreases significantly from neonatal to late infancy and then increases significantly to late childhood and adolescence ($p < 0.05$, FDR corrected). The increase from early childhood to adolescence is also significant ($p < 0.05$, FDR corrected). Thus, effective connectome reduces first from early to late infancy before gradually increasing towards adolescence.

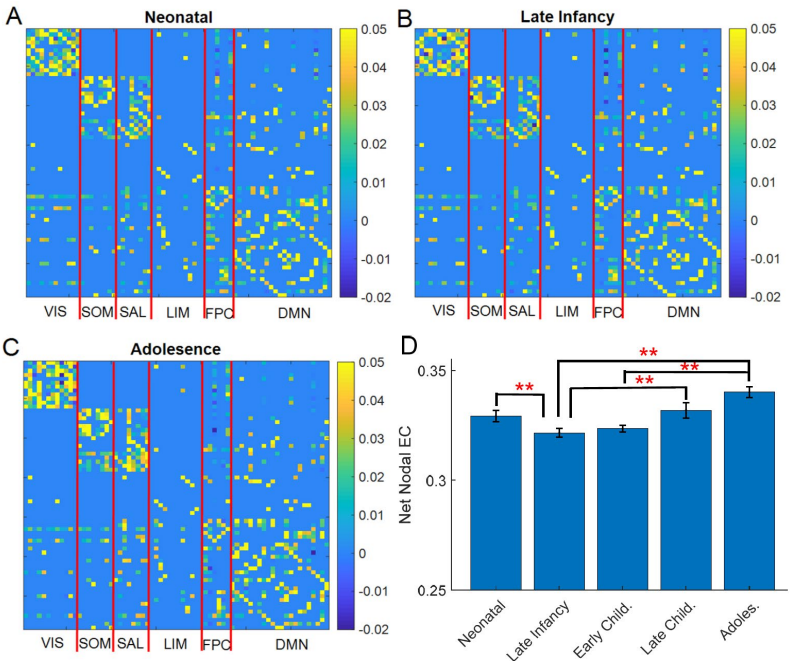

Fig. 1. Evolution of effective connectivity (EC) from infancy to adolescence. Average EC in neonatal (A), late infancy (B) and adolescence (C). (D) Average net nodal EC in different age groups. VIS: visual network; SOM: somatomotor network; SAL: salience network; LIM: limbic network; FPC: frontoparietal control network; DMN: default mode network. Error bars indicate standard errors. Double stars indicate corrected significance ($p < 0.05$).

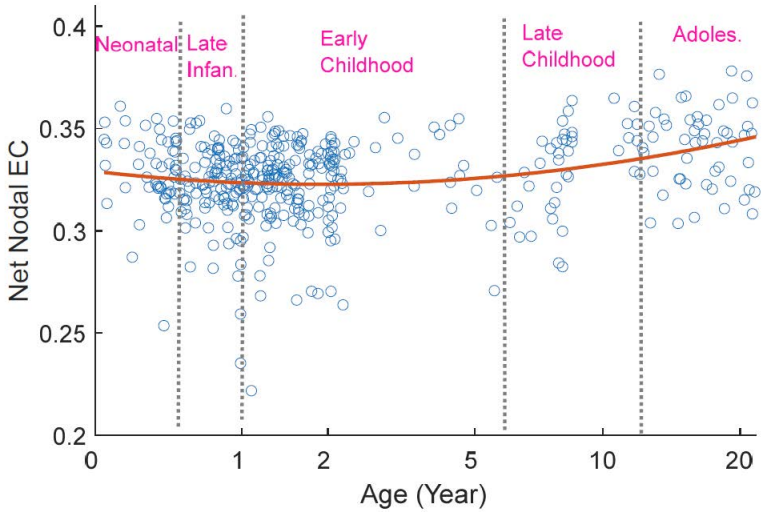

Fig. 2. Developmental trajectory of the mean net nodal EC with age. Each blue dot represents the mean net nodal EC for an individual scan. Age is displayed in log scale.

3.2 Significant Age Effect on Nodal EC

Comparison of the AIC indicates the quadratic model is the best fit model for the mean net nodal EC. The developmental trajectory of the mean net nodal EC among all 68 ROIs is displayed in Fig. 2 where the nodal EC decreases first and then increases with age with the minimal EC at around 2 years old. Linear mixed model indicates significant age effect on the mean net nodal EC ($p < 0.05$, FDR corrected), while there is no significant sex effect on the mean net nodal EC ($p > 0.05$). Application of the linear mixed model on individual net nodal EC shows five brain regions have the most significant age effect on net nodal EC ($p < 0.05$, FDR corrected), including the left and right cuneus, left precuneus, left supramarginal gyrus and right inferior temporal gyrus.

3.3 Coordinated Development of Excitatory and Inhibitory EC

One major advantage of EC over FC is that it allows the characterization of excitatory and inhibitory connectivity separately. The developmental profiles of excitatory (positive) mean nodal EC and inhibitory (negative) mean nodal EC are shown in Fig. 3A, B, respectively. The positive nodal EC decreases slightly from neonatal to late infancy, then increases rapidly to late childhood followed by a slight reduction in adolescence, which parallels the development of the net nodal EC (Fig. 1D) except for the slight decrease from late childhood to adolescence. The inhibitory nodal EC follows a similar trajectory. It increases continuously (i.e., more negative) from neonatal to late childhood followed by a reduction from late childhood to adolescence. As the major developmental change of the excitatory nodal EC is increasing from neonatal to late childhood, the excitatory and inhibitory EC show coordinated developmental profiles.

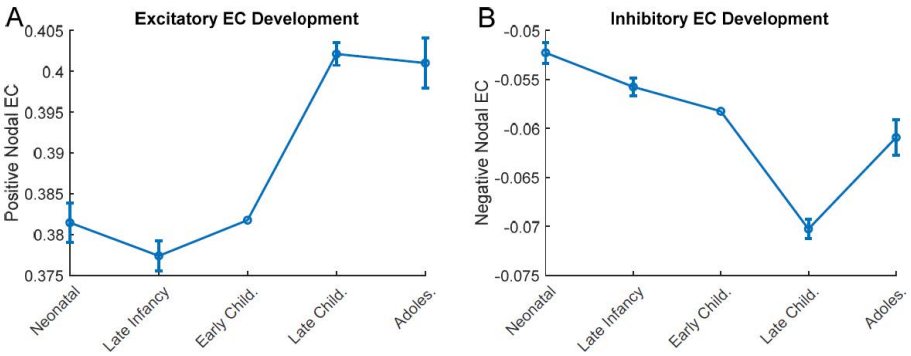

Fig. 3. Developmental profiles of excitatory mean nodal EC (**A**) and inhibitory mean nodal EC (**B**). Error bars indicate standard errors.

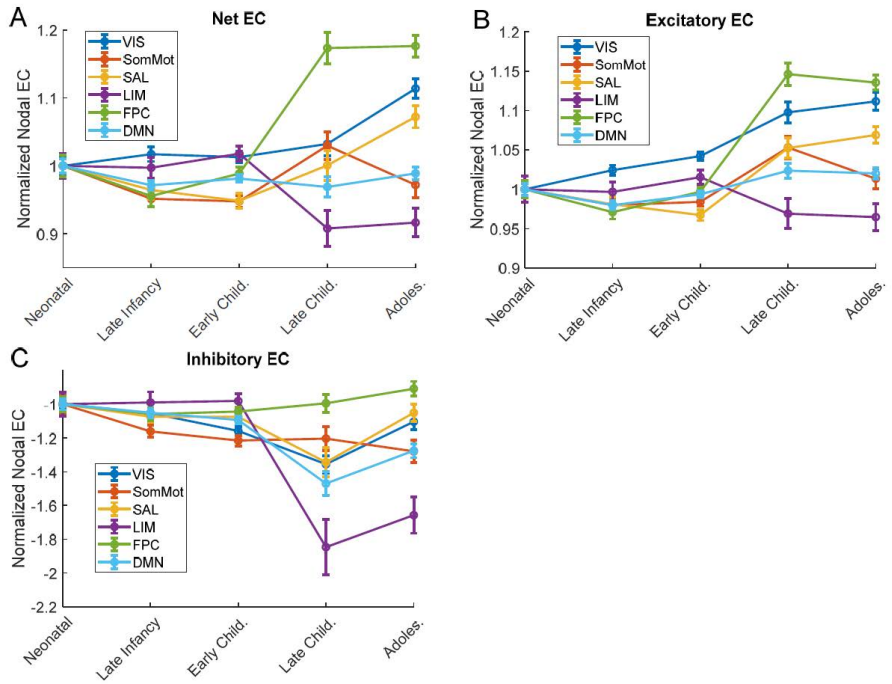

Fig. 4. Network-dependent evolution of nodal EC. Normalized network-averaged net nodal EC (**A**), excitatory nodal EC (**B**), and inhibitory nodal EC (**C**) among different age groups. VIS: visual network; SomMot: somatomotor network; SAL: salience network; LIM: limbic network; FPC: frontoparietal control network; DMN: default mode network. Error bars indicate standard errors.

3.4 Network-dependent Evolution of Nodal EC

The developmental profiles of the average nodal EC among six functional networks are shown in Fig. 4. For the net nodal EC (Fig. 4A), we observe that except for the visual network that shows small increase from neonatal to late infancy, all other networks slightly decrease from neonatal to late infancy and either stay at the same level or return to the original neonatal level in early childhood. From early childhood to adolescence, the frontoparietal control (PFC) network shows the fastest increase followed by the visual network and salience network. Interestingly, the somatomotor network increases from early childhood to late childhood but decreases towards adolescence. The limbic network is the only network that decreases considerably from early childhood to late childhood and adolescence. Decomposition of the mean nodal EC into excitatory (Fig. 4B) and inhibitory (Fig. 4C) components demonstrates that the excitatory EC of the visual network increases continuously from neonatal to adolescence. Thus, the visual network develops first from neonatal to early childhood, while the PFC develops the strongest from early childhood to adolescence. Moreover, the inhibitory nodal EC of most of the networks (except for FPC and somatomotor) increases slightly from neonatal to early childhood followed by a more pronounced increase (i.e., more negative) from early childhood to late childhood before decreasing considerably towards adolescence. Of note, the limbic network shows the largest inhibition increase in nodal EC from early childhood to late childhood.

4 Discussion

Utilizing a high quality rs-fMRI dataset from BCP and HCP-D, we delineated the developmental trajectory of effective connectome from infancy to adolescence for the first time. We showed that the nodal EC follows a nonlinear trajectory which decreases first from neonatal to late infancy and then increases robustly from early childhood to adolescence. Such nonlinear development patterns may represent the complex neurobiological processes that take place during infancy including myelination, synaptogenesis, and axonal and synaptic pruning [2]. Of note, the reconfiguration and reorganization due to sensory exposure could result in retraction of callosal fibers up to 70% in primates [23], which may explain the reduction in nodal EC from neonatal to late infancy. The strong increase in effective connectome from early childhood to adolescence reflects the strengthening of anatomical structures from childhood to adulthood [24], which is also consistent with increased functional connectivity during this period [8]. The enhanced effective connectivity may contribute to elevated functional integration and improved cognitive functions during the transition from early childhood to adolescence. In addition, we revealed the visual network develops first during early years while the FPC network develops the strongest starting early childhood, consistent with early development of sensory systems and late development of association brain systems [2]. Lastly, we observed that the excitatory EC and inhibitory EC develop in parallel in a coordinated fashion, which may lead to relatively stable excitation-inhibition balance during development. Overall, our study represents the first attempt to chart effective connectome from infancy to adolescence, which reveals novel insights into the

nonlinear nature of early brain development. The normative EC reference charts could serve to benchmark individual brain development and aid in the early detection of developmental disorders.

Acknowledgments. This work was supported in part by the United States National Institutes of Health (NIH) through grants R01 MH125479 and R01 EB008374.

Disclosure of Interests. The authors have no competing interests to disclose.

References

1. Sydnor VJ, Larsen B, Bassett DS, Alexander-Bloch A, Fair DA, Liston C, Mackey AP, Milham MP, Pines A, Roalf DR, Seidlitz J, Xu T, Raznahan A, Satterthwaite TD. Neurodevelopment of the association cortices: Patterns, mechanisms, and implications for psychopathology. Neuron **9**(18), 2820-2846 (2021).
2. Nielsen AN, Kaplan S, Meyer D, Alexopoulos D, Kenley JK, Smyser TA, Wakschlag LS, Norton ES, Raghuraman N, Warner BB, Shimony JS, Luby JL, Neil JJ, Petersen SE, Barch DM, Rogers CE, Sylvester CM, Smyser CD. Maturation of large-scale brain systems over the first month of life. Cereb Cortex bhac242 (2022).
3. Gilmore JH, Knickmeyer RC, Gao W. Imaging structural and functional brain development in early childhood. Nat Rev Neurosci **19**(3), 123-137 (2018).
4. Monk C, Lugo-Candelas C, Trumpff C. Prenatal developmental origins of future psychopathology: mechanisms and pathways. Annu Rev Clin Psychol **15**, 317-344 (2019).
5. Fair DA, Cohen AL, Power JD, Dosenbach NU, Church JA, Miezin FM, Schlaggar BL, Petersen SE. Functional brain networks develop from a "local to distributed" organization. PLoS Comput Biol **5**(5), e1000381 (2009).
6. Hwang K, Hallquist MN, Luna B. The development of hub architecture in the human functional brain network. Cereb Cortex. **23**(10), 2380-93 (2013).
7. Bhana A. Middle chilldhood and pre-adolescence. HSRC Press (2010).
8. Fan F, Liao X, Lei T, Zhao T, Xia M, Men W, Wang Y, Hu M, Liu J, Qin S, Tan S, Gao JH, Dong Q, Tao S, He Y. Development of the default-mode network during childhood and adolescence: A longitudinal resting-state fMRI study. Neuroimage **226**, 117581 (2021).
9. Xiao Y, Zhai H, Friederici AD, Jia F. The development of the intrinsic functional connectivity of default network subsystems from age 3 to 5. Brain Imaging Behav **10**, 50–59 (2016).
10. Li G and Yap PT. From descriptive connectome to mechanistic connectome: Generative modeling in functional magnetic resonance imaging analysis. Front Hum Neurosci **16**, 940842 (2022).
11. Friston KJ, Harrison L, Penny W. Dynamic causal modeling. Neuroimage **19**, 1273–1302 (2003).
12. Frässle S, Lomakina EI, Razi A, Friston KJ, Buhmann JM, Stephan KE. Regression DCM for fMRI. Neuroimage **155**, 406–421 (2017).
13. Frässle S, Lomakina EI, Kasper L, Manjaly ZM, Leff A, Pruessmann KP, Buhmann JM, Stephan KE. A generative model of whole-brain effective connectivity. Neuroimage **179**, 505–529 (2018).
14. Frässle S, Harrison SJ, Heinzle J, Clementz BA, Tamminga CA, Sweeney JA, Gershon ES, Keshavan MS, Pearlson GD, Powers A, Stephan KE. Regression dynamic causal modeling for resting-state fMRI. Hum Brain Mapp **42**, 2159-2180 (2021).

15. Howell BR et al. The UNC/UMN Baby Connectome Project (BCP): An overview of the study design and protocol development. Neuroimage **185**, 891–905 (2019).
16. Somerville LH et al. The Lifespan Human Connectome Project in Development: A large-scale study of brain connectivity development in 5–21 year olds. Neuroimage **183**, 456– 468 (2018).
17. Zhang H et al. Infant resting-state FMRI analysis pipeline for UNC/UMN Baby Connectome Project. OHBM, Rome, Italy June 9-13 (2019).
18. Glasser MF et al. The minimal preprocessing pipelines for the Human Connectome Project. Neuroimage **80**, 105-124 (2013).
19. Desikan RS, Ségonne F, Fischl B, Quinn BT, Dickerson BC, Blacker D, Buckner RL, Dale AM, Maguire RP, Hyman BT, Albert MS, Killiany RJ. An automated labeling system for subdividing the human cerebral cortex on MRI scans into gyral based regions of interest. Neuroimage **31**, 968–980 (2006).
20. Yeo BT, Krienen FM, Sepulcre J, Sabuncu MR, Lashkari D, Hollinshead M, et al. The organization of the human cerebral cortex estimated by intrinsic functional connectivity. J Neurophysiol **106**, 1125–1165 (2011).
21. Bethlehem RAI, Seidlitz J, White SR, Vogel JW, Anderson KM, Adamson C, et al. Brain charts for the human lifespan. Nature **604**, 525-533 (2022).
22. Li G, Liu Y, Zheng Y, Li D, Liang X, Chen Y, Cui Y, Yap P, Qiu S, Zhang H, Shen D. Large-scale dynamic causal modeling of major depressive disorder based on resting-state fMRI. Hum Brain Mapp **41**, 865-881 (2022).
23. LaMantia AS, Rakic P. Axon overproduction and elimination in the corpus callosum of the developing rhesus monkey. J Neurosci **10**(7), 2156-2175 (1990).
24. Supekar K, Uddin LQ, Prater K, Amin H, Greicius MD, Menon V. Development of functional and structural connectivity within the default mode network in young children. Neuroimage **52**(1), 290-301 (2010).